

**Radar Observations of Precipitation and Airflow on the Mediterranean Side  
of the Alps: Autumn 1998 and 1999**

*Link to publication version:*  
*Quart. J. Roy. Meteor. Soc., 127, 2537-2558.*

Robert A. Houze, Jr.,<sup>1</sup> Curtis N. James<sup>2</sup> and Socorro Medina

Department of Atmospheric Sciences  
University of Washington  
Seattle, Washington USA

Resubmitted  
*Quarterly Journal of the Royal Meteorological Society*

June 2001

---

<sup>1</sup> Corresponding author address: Professor R. A. Houze, Jr., Department of Atmospheric Sciences, Box 351640, University of Washington, Seattle, WA, 98195-1640, USA. E-mail: houze@atmos.washington.edu

<sup>2</sup> Present address: Embry-Riddle Aeronautical University, Meteorology Lab, 3200 Willow Creek Road, Prescott, AZ 86301-3720. E-mail: jamesc@pr.erau.edu

## SUMMARY

This study constructs and analyzes composite three-dimensional fields of Doppler-radar observed radial velocity and reflectivity for all precipitation events occurring in the Lago Maggiore region on the Mediterranean side of the Alps during autumn 1998 and 1999. Mean patterns for the two years are in close agreement with each other. The radar data are consistent with previous rain gauge studies in showing that the rain was heaviest over the lower windward slopes and decreased toward higher terrain. The three-dimensional reflectivity fields show that precipitation growth occurred mainly at low altitudes. The composite radar data show that the precipitation was most intense when the mean flow around the 2-km level was southerly or southeasterly, i.e., when the mean flow was most perpendicular to the Alpine barrier.

Sounding data from Milan indicated the Froude number of the flow upstream of the Lago Maggiore region. When the Froude number was high, the flow proceeded directly up and over the terrain of the lower Alpine slopes. Under these unblocked conditions, the low-level flow (including the layer from the surface to 2-km MSL) rose directly up and over the terrain, and the precipitation was greatly enhanced over the lower windward slopes and over the portions of the Po Valley just upstream of the mountains. Under unblocked conditions, the precipitation enhancement only extended a short distance (a few tens of kilometers) upstream of the Alps.

When the upstream Froude number computed from the Milan sounding was low (blocked conditions), the Doppler radial velocities indicated that the low-level flow (in the layer below 2-km MSL) turned cyclonically as it approached the Alpine barrier, instead of rising over the terrain. The composite radar reflectivity data showed less precipitation enhancement directly over the windward slope but in contrast to the unblocked case showed that the precipitation was enhanced 140 km or more upstream of the terrain. Evidently, the low-level flow began rising far in advance of the barrier in blocked conditions.

The 1998-1999 autumn data sample further indicates the relative roles of wind speed and stability, which are combined in the Froude number. When the wind speed upstream was strong ( $> 8 \text{ m s}^{-1}$ ), significant precipitation enhancement occurred on the windward slope of the Alps in the Lago Maggiore region, regardless of the static stability. However, the enhancement was far greater under unstable conditions. When the wind speed was weak ( $< 8 \text{ m s}^{-1}$ ), the precipitation was generally near or below average, except when the stability was low and some patchy enhancement occurred over the Po Valley just upwind of the Alps.

A diurnal precipitation maximum occurred in the early morning hours (0700-1000 LST), possibly where down-valley flow converged with synoptic-scale up-valley flow.

## 1. INTRODUCTION

The European Alps are notorious for heavy rains and floods (Lionetti 1996; Buzzi *et al.* 1998; Doswell *et al.* 1998; Ferretti *et al.* 2000; Rotunno and Ferretti 2001). These events occur primarily in the autumn on the Mediterranean side of the Alps, when moist Mediterranean air ahead of baroclinic waves impinges on the barrier. Orographic air motions modify the baroclinic circulation to produce locally heavy and persistent rain, which runs off rapidly in deep rocky narrow river valleys emptying into the Po Valley of northern Italy. The high Alpine mountain barrier juxtaposed with the Mediterranean moisture source make the region a natural laboratory for studying orographic precipitation. The Mesoscale Alpine Programme (Bougeault *et al.* 2001) took advantage of these characteristics of the Alps by organizing a field program to investigate orographic precipitation on the Mediterranean side of the Alps in autumn 1999.

Frei and Schär (1998) have analyzed data from rain gauges to map the mean pattern of precipitation over the Alps. Figure 1 shows their pattern for the autumn season. Prominent mesoscale maxima of rainfall accumulation occur on the southern slopes of the Alps collocated with indentations or concavities in the terrain. These maxima are mesoscale in the sense that they are much smaller than the whole Alpine massif yet much larger than individual river valleys. Two of these prominent mesoscale rainfall maxima are at  $8.5^{\circ}\text{E}$ ,  $46.2^{\circ}\text{N}$  and  $13.8^{\circ}\text{E}$ ,  $46.2^{\circ}\text{N}$ . At each location, the 80-m MSL terrain contour (thick line) curves inward. The mesoscale rainfall maximum outlined by the rectangle in Fig. 1 is the region we examine in this study.

Figure 2 shows details of the topography within the region of the rectangle. At smaller scales, within each mesoscale maximum, the multiple ridges, peaks and river valleys further modify precipitation and runoff. The mesoscale indentations in the terrain evidently focus the large-scale moist flow over the barrier so as to maximize rain in these regions. The effects on the flow at these scales are probably in the category of quasi-balanced adjustments of the large-scale flow to the curvature of the terrain barrier. The smaller-scale peaks, ridges and river valleys produce more localized effects, where the Coriolis force is negligible.

One of the scientific objectives of the MAP Special Observing Period (SOP), conducted from 7 September through 15 November 1999 in the region shown in Fig. 2, was to investigate how the Alpine barrier affects precipitation on a descending cascade of scales from the scale of the entire barrier, to the mesoscale indentations of the barrier, to individual ridges, peaks and river valleys (Houze *et al.* 1998). For the SOP, seven ground-based research radars and two aircraft-borne radars collected data on the Mediterranean side of the Alps. The ground-based radar network was configured to sample the mesoscale precipitation within the area enclosed by the rectangle in Figs. 1 and 2. For the remainder of the paper we will refer to this area as the Lago Maggiore region.

We examine rain events that occurred in the Lago Maggiore region during autumn 1998 and 1999, the year before and the year of the MAP SOP. The primary data of the study is the Swiss Meteorological Institute's Doppler weather radar located at the top of Monte Lema (altitude = 1.63 km, Fig. 2). This radar was the only MAP radar that operated in the Lago Maggiore during both years. In addition we use data taken during the 1999 MAP SOP by the

French RONSARD and the U.S. NCAR S-Pol radars (also located in Fig. 2). We take advantage of the radars' ability to provide four-dimensional fields of radar reflectivity (a metric of the precipitation intensity) and radial velocity (an indicator of the airflow producing the precipitation) in high resolution over the whole autumn season. We analyze the data climatologically (statistically) rather than by cases to obtain the most general picture possible of the airflow and precipitation processes at work in this critical region. We make use of sounding data to characterize the upstream conditions and to stratify the data by Froude number, wind speed and stability. Specifically, the objective of this study is to use superposed epoch (i.e. composite) analysis of the radar data to help establish the relative importance of these parameters in determining the orographic modification of the precipitation produced by the storms affecting the Lago Maggiore region.

## 2. DATA AND METHODS OF ANALYSIS

### (a) *The Monte Lema radar*

Joss *et al.* (1998) describe the Monte Lema C-band radar in detail. It is an operational radar, and the elevation angle (tilt) sequence is fixed and includes 20 tilts per 5-min period (Fig. 3). The reflectivity data undergo rigorous quality control within the radar processor. A decision tree algorithm consisting of a reflectivity threshold, a wide-band noise threshold, a Doppler velocity threshold, two statistical filters, a vertical reflectivity gradient test and a clutter map was incorporated to classify echoes as either clutter, system noise or precipitation. The technique removed virtually all of the reflectivity gates containing noise or terrain backscatter that could adversely affect statistical computations in this study. One notable exception occurred on 21 October 1999 (IOP 8 of MAP), when there was a persistent stable layer of air near the surface, and the lowest beam intercepted one mountain peak in northern Italy. This one case affected the reflectivity statistics at this point in 1999, as will be pointed out in Sec. 3(b). Nevertheless, as with other radars, terrain shadowing, bright band contamination, increasing sample volume size with range, attenuation and wet radome effects are potential sources of error when interpreting the data (Joss *et al.* 1998; Doviak and Zrnić 1993; Houze 1993).

The Monte Lema radar operates with a Nyquist velocity of only  $8.27 \text{ m s}^{-1}$ . Consequently, the radial velocity field contained extensive aliasing, which occurs whenever the magnitude of the radial component of the wind exceeds the Nyquist velocity (Doviak and Zrnić 1993). Since the data set we use in this study contains over 10,000 individual three-dimensional volumes of radar data, it was impractical to dealias the data by hand. We therefore developed and used a new software package called Four-Dimensional Dealiasing (4DD), an efficient dealiasing algorithm, which was used in real time during the MAP SOP (James and Houze 2001). 4DD successfully dealiased the radar volumes with only occasional errors. Even in extreme events, these errors were generally very localized. They were so few as to have a minimal effect on the statistical results of this study.

We consider data taken by the Monte Lema radar during all precipitation events in the Lago Maggiore region from 1 September through 30 November 1998 and from 7 September through 15 November 1999. Three-dimensional volumes of radar data were recorded every 5 min. Following four-dimensional dealiasing, the time interval between volumes was increased

from 5 min to 1 h to reduce the autocorrelation between volumes and ease data storage requirements. The result was a downsizing of the data archive from more than 10,000 radar volumes for the two seasons to 554 volumes for 1998 and 598 for 1999, for a total of 1152 volumes. The remaining volumes were then bilinearly interpolated to a Cartesian grid with a resolution of  $2 \text{ km} \times 2 \text{ km} \times 0.5 \text{ km}$  using NCAR's SPRINT software (Mohr and Vaughan 1979) and finally converted to Unidata's Network Common Data Format (NetCDF) for visualization (James *et al.* 2000). Radar-data interpolation smoothes noise and facilitates computations with the data. Figure 3 superimposes the interpolation grid on the vertical cross-sectional area of the Monte Lema radar scans.

The Monte Lema radar antenna is located at an altitude of 1.63 km MSL. Figure 3 shows that the lowest scan is generally above 1.5 km. Therefore the 2-km level is about the lowest available grid level that can be obtained using bilinear interpolation. In addition, the bilinear interpolation cannot produce an estimate of the conditions beyond a range of about 60 km. Therefore, we consider results for the Monte Lema radar only at or above the 2-km level and only out to a range of 60 km.

*(b) The RONSARD and S-Pol radars*

During the 1999 MAP season, two other scanning Doppler radars were installed at fixed locations at lower altitudes over the Po Valley (Bougeault *et al.* 2001). The NCAR dual-polarization S-Pol radar ([linus.atd.ucar.edu/rsf/spol/spol.html](http://linus.atd.ucar.edu/rsf/spol/spol.html)) and the French RONSARD radar (Chong *et al.* 2000) were at the locations shown in Fig. 2. The S-Pol was at an altitude of 0.28 km MSL, and the RONSARD was at 0.155 km MSL. After reducing the data to 1-hour resolution, 320 radar volumes remained for S-Pol and 213 for RONSARD. Results from these radars supplement the Monte Lema results by providing information at altitudes below 2 km. The RONSARD also provides information on the radial velocity and reflectivity patterns over the Po Valley, south of the Lago Maggiore region.

*(c) Calculations based on the radar data*

It has been shown that sampling over long time periods, such as the autumn seasons considered in this study, greatly reduces the large uncertainties in radar rainfall estimates by removing the scatter of individual measurements (Joss and Waldvogel 1990; Cain and Smith 1976). We therefore convert horizontal patterns of radar reflectivity to patterns of rain rate to attach a meteorological unit to the reflectivity values. However, this paper does not require highly precise estimates of rainfall rates or amounts. Rather, it is the variability of the rates (or reflectivity values) in time, in space and by meteorological epoch that are the focus of this study. In vertical cross-sections we display the data in reflectivity units since rain rate has no meaning above the  $0^\circ\text{C}$  level.

We obtain the seasonal mean rainfall rate and radial velocity during all storm events in the 1998 and 1999 MAP seasons by averaging the radar-derived rainfall rate and radial velocity fields. The rainfall rate was estimated using the Marshall and Palmer (1948) *Z-R* relation:

$$Z = 200R^{1.6}, \quad (1)$$

where  $Z$  is the equivalent reflectivity in  $\text{mm}^6 \text{m}^{-3}$  and  $R$  is the rainfall rate in  $\text{mm h}^{-1}$ . The rain rate and radial velocity calculations treated missing echoes differently. We assumed that missing reflectivity meant that no precipitation was occurring, whereas a similar assumption could not be made with missing radial velocity gates. Therefore, the mean rain rate  $\bar{R}$  and radial velocity  $\bar{v}$  were computed as

$$\bar{R} = \frac{\sum_{i=1}^N R_i}{N} \quad (2)$$

and

$$\bar{v} = \frac{\sum_{j=1}^n v_j}{n}, \quad (3)$$

where  $N$  is the total number of volumes, and  $n (\leq N)$  is the number of volumes with available radial velocity values at the grid point in question. From (2), it is evident that maxima in the mean rain rate field indicated regions where the precipitation was either more frequent, more intense or both. To remove some of this ambiguity, a third field called the precipitation frequency was calculated and defined as the percentage of the total volumes in which reflectivity  $\geq 13 \text{ dBZ}$  ( $\sim 0.16 \text{ mm h}^{-1}$ ) was observed at each grid point.

In order to investigate the sensitivity of precipitation to a given variable, superposed epoch analyses (e.g. Reed and Recker 1971) were performed. This analysis extracted all volumes from the archive whose time stamps (beginning time of data recorded in a volume) corresponded to *epochs*, defined by some specified condition. Then, the mean rainfall rate, radial velocity and standard deviations were computed at each grid point in the sample of extracted volumes.

#### (d) Statistical testing

To indicate the statistical significance of our maps of rainfall rate and radial velocity over seasons and individual epochs within seasons we have computed a standard  $t$ -statistic and exercised the Student's  $t$ -test at each pixel in the domain (Appendix). The  $t$ -statistic was plotted as a horizontal field for each map that we constructed. The most informative  $t$ -statistic maps are included and will be discussed where relevant in Sec. 4.

#### (e) Variables characterizing the upstream flow

We define meteorological epochs within the autumn season primarily by characteristics of the upstream flow. The flow into the region of precipitation observed by radar was sampled every six hours by radiosonde measurements from the Milano-Linate Airport (labeled "Milano" in Fig. 2). From these data we calculated wind direction, wind speed, static stability and Froude number to characterize the environment immediately upstream of the radar-observed area. The values of these variables defined data subsets used in the superposed epoch analysis. Each variable was represented by its average value within the 925-700 hPa layer (corresponding roughly in altitude to 0.75-3 km MSL) in the sounding. If no sounding was available within 3 h

of a radar volume time stamp, the volume was not used for those superposed epoch analyses that required sounding information. Sounding information was available for only 480 of the 554 radar volumes for the 1998 MAP season, for 549 of the 598 Monte Lema radar volumes and for 190 of the 213 RONSARD radar volumes for the 1999 season.

The Froude number is  $Fr=U/(NH)$ , where  $U$  is the upstream flow speed,  $N$  is static stability and  $H$  is the height of the mountain barrier. We let the terrain height  $H= 2.5$ -km MSL, the characteristic elevation of mountain passes along the north side of the Lago Maggiore region. We performed superposed epoch analyses based on the flow strength, static stability and Froude number for southerly and southeasterly flow events (specifically, those in which the direction of the mean flow in the 925-700 hPa layer was between 112.5 and 202.5° azimuth). The Brunt-Väisälä frequency was computed using finite differences over the 925-700 hPa layer. We will use the moist Brunt-Väisälä frequency (Durran and Klemp 1982). This choice is consistent with the fact that we are considering only cases of precipitation seen by radar. We assume that even if the upstream Milano sounding was less than saturated the air was saturated by the time it was producing rainfall over the Alps. Experiments assuming dry or moist Brunt-Väisälä frequency based in a humidity threshold (e.g. Mass and Ferber 1990) led to erratic results.

### 3. OVERALL AVERAGE PATTERNS OF RADIAL VELOCITY AND REFLECTIVITY

#### *(a) Mean radial velocity pattern*

Figures 4(a) and (b) show the Monte Lema radar's mean radial velocity field for both 1998 and 1999. The mean radial velocity field for the 1998 season (Fig. 4(a)) indicates that the prevailing wind direction at 2-km MSL was south-southeasterly and its magnitude was 4-6 m s<sup>-1</sup>. The 1999 season mean radial velocity (Fig. 4(b)) compares well with that of 1998, except that the flow was slightly more intense (6-8 m s<sup>-1</sup>) and had a slightly more easterly direction. For 1999, the RONSARD and S-Pol radars deployed for MAP provided low-level radial velocity data not available in the Monte Lema data. The mean radial velocity observed by the RONSARD radar during autumn 1999 at an altitude of 2 km (Fig. 4(c)) was similar to that of Monte Lema at 2 km. The wind direction shifted to east-southeasterly at 1 km (Fig. 4(d)) and to easterly at 0.5 km (Fig. 4(e)).

A change from easterly to southerly with increasing height at low levels was also a characteristic of the Piedmont flood on the Mediterranean side of the Alps in November 1994 (Buzzi *et al.* 1998; Doswell *et al.* 1998; Ferretti *et al.* 2000; Rotunno and Ferretti 2001).

The predominance of southeasterly flow at 2 km, as indicated by the radial velocity fields in Fig. 4(a-c), agrees with a longer-term rawinsonde climatology compiled by Kappenberger and Kerkmann (1997) for autumn precipitation events over the Lago Maggiore region. They found that the synoptic setting most favorable for precipitation over the Lago Maggiore region was amid southwesterly flow at 500 hPa, ahead of an approaching upper-level trough, while at 850 hPa the wind directions ranged from east through south to southwest. Inspection of the average radial velocity field at higher levels (not shown) indicates that the wind veered with height during precipitation events in the Lago Maggiore region, becoming southwesterly at 5-km MSL, consistent with Kappenberger and Kerkmann's climatology.

*(b) Mean radar reflectivity pattern*

Figure 5(a) and (b) shows the mean rainfall rate field derived from the Monte Lema radar data for the 2-km MSL level for September-November 1998 and 1999. The rain rate fields for the two years are consistent with each other, which indicates that the MAP SOP comprised a data set representative of the autumn Alpine climatology. The spot of abnormally high reflectivity ~19 km northwest of the radar in the 1999 reflectivity map (Fig. 5b) was produced by anomalous propagation in IOP8, as mentioned in Sec. 2a. This point was the only one in either year that was obviously affected by clutter. The influence of this clutter is evident in several of the figures to be discussed below; this point should be ignored.

The rain rate fields in 1998 and 1999 are also consistent with the rain-gauge-based climatology of Frei and Schär (1998; Fig. 1) but provide additional local detail plus three dimensionality. A vertical cross-section through the mean reflectivity field for the 1998 season (Fig. 5(c) and (e)) is consistent with the results of Frei and Schär (1998) in that the maximum precipitation occurred over the windward slopes of the Alpine range rather than over the highest terrain. The melting level was nearly always between 2 and 3 km. The radar bright band may have caused the altitude of maximum reflectivity implied by radar to be located somewhat higher than its actual location on the windward slope, but still well below the maximum height of the Alpine barrier (~4 km). The maximum in the vertical cross-section occurred between  $x = 25$  and  $x = 40$  km on the horizontal axis. Terrain clutter may have caused some slight overestimation of the radar echo intensity as a result of residual clutter or side lobe echoes in this region; however, the Swiss Meteorological Institute's intensive quality control of the raw data (Sec. 2(a)) all but eliminates this possibility. Echoes occurring downstream, over the highest peaks ( $\sim x = 10$  km) and upstream over the Po Valley, were of consistently lower intensity. The vertical cross-section of precipitation frequency (Fig. 5(d) and (f)), defined as the percentage of volumes in which the reflectivity equaled or exceeded 13 dBZ, was also maximum on the lower windward slopes, where the average reflectivity (Fig. 5(c) and (e)) was maximum; hence this maximum was not a transient feature but a robust characteristic throughout the season.

Since the S-Pol radar's beam was not blocked at low levels as much as that of the Monte Lema radar, the vertical cross-sections of reflectivity in Fig. 5(e) and (f) further show how the mean echo pattern extended below 2 km down to near the surface of the terrain. The height of the maximum reflectivity (slightly above ~2 km) was the same in both years. By examining the individual storms making up the seasonal mean pattern, we determined that sometimes the precipitation over the windward slopes was purely stratiform, while in other cases the convective cells were embedded in a stratiform background. In the stratiform cases, the maximum reflectivity at 2-3 km was evidently determined by melting; the 0°C level was usually at 3 km, sometimes as low as 2 km. When the stratiform precipitation was enhanced by embedded convective cells, the reflectivity pattern showed cells with maximum intensities in the 2-4 km altitude range against the background of stratiform radar echo. The cellular convective echo maxima were likely produced by coalescence of drops and/or riming growth of the precipitation particles (Houze and Medina 2001). The echo pattern in Fig. 5(e) was the combination over the whole season of the stratiform and convective precipitation mechanisms, with a bright band

extending across the section at the 2-3 km level, out over the Po Valley, with embedded mean cells over the lower Alpine terrain, where the embedded convective echoes preferred to occur.

In the 1999 S-Pol data, the maximum echo was shifted ~10 km to the south-southeast (Fig. 5(e)), a feature that was also seen in the 1999 Monte Lema data (not shown). The precipitation frequency seen on S-Pol in 1999 (Fig. 5(f)) was also consistent with the pattern seen in the 1998 Monte Lema observations, and also shifted to the south-southeast.

The vertical cross-sections of reflectivity (Fig. 5(c) and (e)) both indicate that the maximum reflectivity consistently occurs at low altitude, below ~4 km MSL. This altitude is approximately the height of the highest terrain downstream. This persistent feature of the echo pattern indicates that the precipitation particles form, grow and fall out quickly and efficiently over the lower slopes of the Alpine barrier, with most of the precipitation particle growth occurring at low levels. The height of the 0°C isotherm in this season was typically 3-km MSL or lower. The echo maxima extend above this height. Therefore, the precipitation growth mechanisms are not entirely warm coalescence of liquid drops. Ice evidently also plays a role in the growth. Polarimetric measurements with the S-Pol radar in MAP are consistent with these inferences (Houze and Medina 2001). Further study of the MAP data will focus on identification of these low-level growth mechanisms over the lower windward slopes of the terrain.

Since the autumn 1998 and 1999 seasons are in general agreement, we have merged the data for the two years in the analyses described in the remainder of this paper.

#### 4. REFLECTIVITY AND VELOCITY PATTERNS BY EPOCH

##### *(a) Rain distribution as a function of direction of impinging flow*

As mentioned in Section 1, the terrain curves inward over the Lago Maggiore region. Figure 6 indicates the influence of the concave shape of the topography on the precipitation in relation to the upstream wind direction. The individual panels of this figure present the radar data for autumn 1998 and 1999 according to the average wind direction in the 925-700 hPa layer, as computed from the Milano soundings (Sec. 2(e)). For each wind-direction category (east, southeast, south, and southwest), the panels on the left show the distribution of radar-derived rain rate while the panels on the right show the statistic of the rain pattern (computed as described in Sec. 2(d) and the Appendix). Each panel also shows the 800-m MSL topographic contour. This contour indicates both the fine-scale pattern of ridges and valleys in the lower portion of the Alps and the broader outline of the mesoscale convex indentation of the Alps surrounding the Lago Maggiore region (cf. Figs. 1 and 2). The contour lies generally east, north, and west of the Monte Lema radar, with the lowland region of the Po Valley lying to the south. Thus, winds over this region from the east, southeast, south, and southwest each encounter rising terrain.

Figure 6a shows the rain rate field at 2 km for the easterly flow cases (wind direction between 67.5 and 112.5°), which favor upslope enhancement of precipitation over the western slopes of the mountains surrounding the area covered by the radar. The statistical significance of this result is shown by the field of the  $t$ -statistic of the rain rate at the 2-km level (Fig. 6(b)). The red areas, where  $t > 1.96$ , indicate where the sample mean is significantly above the seasonal

mean. Blue areas, where  $t < -1.96$ , indicate where the sample mean is significantly below the seasonal mean. Over most of the domain, the precipitation rate was not significantly different from the seasonal climatology. Rates were significantly above the seasonal mean over some regions to the west, where the flow was upslope, and significantly below over a few slopes of the eastern side, where the flow was downslope. The composite for southeasterly flow (112.5-157.5°, Fig. 6(c)) shows intense precipitation over most of the domain with a statistically significant precipitation increase over the western slopes and over the Po Valley (Fig. 6(d)). The cases with southerly flow (157.5-202.5°, Fig. 6(e) and (f)) had intense, significantly increased precipitation over all the lower slopes of the Lago Maggiore area. Comparison of figure panels 6(c) and (e) indicates that both southeasterly and southerly flow produced large orographic enhancement of rainfall on the lower slopes of the Alps, with the latter providing the strongest upslope component. In southwesterly flow, precipitation was below the seasonal mean, especially in the western portion of the radar domain, evidently because of downslope flow (Figs. 6(g) and (h)).

(b) *Froude number*

From section 4(a) it is evident that the southeasterly and southerly cases are associated with the most intensely orographically enhanced precipitation. Therefore, we will restrict the Froude number analysis to cases within these two epochs.

The Froude number combines the influences of stability, wind speed and terrain height. It indicates whether or not the flow has enough kinetic energy to rise over the barrier (Durrán 1990; Chapter 12 of Houze 1993). It therefore suggests whether or not the orographic lifting will occur directly over the terrain or upstream. High Froude number flow rises easily over a mountain barrier and robust upslope flow occurs, which can enhance precipitation over the windward side of a mountain barrier. When low Froude number flow is blocked by the terrain, lifting and enhancement of rainfall can occur upstream of the barrier (e.g. Grossman and Durrán 1984).

Figure 7(a) shows the fields of rain rate and  $t$ -statistic at the 2-km level for the Froude number composite analyses. These patterns contain all radar data obtained when the flow into the Lago Maggiore region, as measured by the Milano sounding, was southeasterly or southerly and not blocked ( $Fr > 1$ , Fig. 7(a) and (b)) and blocked ( $Fr < 1$ , Fig. 7(c) and (d)). The  $t$ -statistic calculations show that when the Froude number was high, the precipitation rates over the foothills, lower slopes and western Po valley were significantly stronger.

When the Froude number was low, the precipitation rates were very close to the climatology, with a suggestion of blocking far upstream, near the southeast corner of the radar domain at a range of about 80 km from the radar. The Alpine crest is located 60 km to the north and northwest of the radar site. The characteristic horizontal scale over which the effects of blocking occur in the case of low Froude-number flow is the Rossby radius of deformation, or

$$L_R = NHf^{-1}, \quad (4)$$

where  $N$  is the moist Brunt-Väisälä frequency and  $H$  is the characteristic barrier height. The average value of  $N$  was about  $0.008 \text{ s}^{-1}$  when the Froude number was  $< 1$ . Using the same value of  $H$  as for the Froude number calculations (2.5 km) and  $f = 1.05 \times 10^{-4} \text{ s}^{-1}$  for 46°N latitude,  $L_R$

$\approx 190$  km. The occurrence of upstream enhancement at a distance of 140 km of the barrier crest is thus consistent with theory.

If the upstream Froude number computed from sounding data truly indicates whether or not the low-level flow is blocked, we would expect the radial velocity field observed by radar to be consistent with relatively unimpeded upslope flow in the high Froude number cases, as well as with blocking in the low Froude number cases. The lowest level we can examine in the Monte Lema radar data is 2-km MSL (Sec. 2(a), Fig. 3). The flow direction at the 2-km level tended toward a more southerly direction in the high Froude number cases (Fig. 8(a)) and toward a more southeasterly direction in the low Froude number cases (Fig. 8(b)). This directional difference would be consistent with the impinging flow at higher Froude number turning cyclonically as it approached the barrier, as would be expected in a blocking scenario. However, it is only a slight directional difference. Also, the strength of the flow is comparable for the two cases. The effect of blocking was apparently felt more strongly at levels below 2 km.

The RONSARD radar (Sec. 2(b)) was able to observe the radial velocity at altitudes below 2 km because of its location in the lowlands of the Po Valley. The 1999 data from RONSARD show that the flow turned sharply cyclonically from east-southeast at high Froude number (Fig. 9(a)) to northeasterly at low Froude number (Fig. 9(b)). Again, this behavior is consistent with the blocking implied by the precipitation patterns in Fig. 7.

Because of its more southern location (Fig. 2) RONSARD radar could see further upstream over the Po valley than could the Monte Lema radar. Therefore, it can be used to investigate the upstream blocking for the  $F < 1$  cases suggested by the Monte Lema radar in Fig. 7(d). Froude number composites of the RONSARD rain rate data (Fig. 10) show enhanced precipitation over the Po valley for  $F < 1$  cases (cf. Fig. 10(a) and (d)). The area of red shading 60 km to the south of RONSARD on the  $t$ -statistic analysis of the rain rate for the  $F < 1$  case (Fig. 10(e)) indicates the statistical significance of the blocking. A vertical cross-section of the RONSARD data along the red line in Fig. 10(a) shows that the precipitation frequency over the Po plain was considerably higher for  $F < 1$  cases.

The Froude number  $Fr = U/(NH)$ , and hence the tendency toward blocking or not, depends on both strength and stability of the flow. To separate these two influences, we subdivided the Froude number composites according to the wind speed (Fig. 11). The cases with upstream wind speed  $> 8$  m s<sup>-1</sup> had the heaviest precipitation on the lower windward slopes of the Alps, especially northwest of the radar (Fig. 11(c) and (g)). We calculated mean upstream winds speed  $U$  and moist Brunt-Väisälä frequency  $N$  for all cases. The upstream wind speeds for the two strong flow cases were comparable (11 m s<sup>-1</sup>), hence any difference in the patterns was due to the stability. Very stable cases constitute the  $F < 1$  strong-flow epoch ( $N = 8.7 \times 10^{-3}$  s<sup>-1</sup>) and thus produce the blocking signal seen as the red (statistically high) area upstream in the  $t$ -statistic field (Fig. 11(h)). Much less stable cases constitute the  $F > 1$  strong-flow composite ( $N = 1.0 \times 10^{-3}$  s<sup>-1</sup>), and the airstream easily rose over the terrain. The  $t$ -statistic showed significantly enhanced rain rate both over and out to about 40 km upstream of the lower slopes of the Alps (red area in Fig. 11(d)).

In contrast to the strong flow cases, the weak flow composites (upstream wind speed 0-8 m s<sup>-1</sup>) have very little precipitation (Figs. 11(a) and (e)). The corresponding *t*-statistic fields indicate that the precipitation over the lower slopes of the Alps was significantly suppressed in these cases (see the blue patches over the lower slopes in both Fig. 11(b) and (f)). The mean wind speed for the two weak-flow regimes was comparable (~5.5 m s<sup>-1</sup>). The extremely low mean stability for the higher Froude number ( $F > 1$ ) weak-flow case ( $0.2 \times 10^{-3} \text{ s}^{-1}$ ) evidently accounted for isolated patchy (probably convective) precipitation over the Po Valley just upstream of the slopes (Fig. 11(a) and (b)). The lower Froude number ( $F < 1$ ) weak flow case (Fig. 11(e)) was very stable ( $N = 7.6 \times 10^{-3} \text{ s}^{-1}$ ) and it produced barely any precipitation.

### (c) Diurnal cycle

Figure 12 shows the total radar-estimated rainfall over the Lago Maggiore region (as defined in Fig. 2) for each hour of the day for autumn 1998 and 1999. A prominent maximum between 0700-1000 LST (0600 and 0900 UTC) occurred in 1998. A maximum occurred during the same time of day in autumn 1999, but it was not as prominent. It is possible that this morning maximum was a sampling fluctuation of these two particular years. However, a physical basis might exist for such a maximum. In autumn 1999, during several MAP Intensive Observing Periods, the mobile Doppler on Wheels (DOW) radar was deployed in the Toce and Ticino River valleys in the Lago Maggiore region. During stable upslope flow events, the DOW observed persistent return flow within the valley in a shallow surface layer less than 2-km deep (Steiner *et al.* 2000; Houze *et al.* 2000). Airborne Doppler radar in MAP also show this down valley flow (Bousquet and Smull 2001). This down-valley flow could have been strongest when the atmosphere was most stable (e.g., in the early morning). One could speculate that as outflow from the valleys emptied into the Po Valley it converged with the synoptic-scale flow and thus enhanced the upward air motion and precipitation within the Lago Maggiore region.

## 5. CONCLUSIONS

During the autumn season in the Lago Maggiore region heavy rains and floods can occur when baroclinic waves bring Mediterranean air into northern Italy at low levels. Whenever this air impinges on the Alpine massif there is the potential for a major rain or flood event. Seasonal climatology of Doppler-radar data for the autumn seasons of 1998 and 1999 document detailed three-dimensional characteristics of the precipitation structure and accompanying airflow. Radar reflectivity and Doppler radial velocity patterns observed in the two seasons are in close agreement with each other. One important implication of this result is that the MAP season (Bougeault *et al.* 2001) was generally representative of autumn rainfall on the Mediterranean side of the Alps.

Consistent with previous studies of rain gauges in the Alps (Frei and Schär 1998), the radar reflectivity was generally strongest over the lower windward slopes and decreased toward higher terrain. Vertical cross-sections of the mean three-dimensional reflectivity patterns for both years show that precipitation generally developed at low altitudes, with most of the precipitation growth occurring at altitudes below the Alpine crest. We suggest that coalescence and/or riming led to rapid particle growth and fallout at low levels. This behavior would be consistent with the findings of previous studies of orographic precipitation. Hobbs *et al.* (1973) and Hobbs (1975)

concluded, both theoretically and empirically, that precipitation particle growth by riming at low levels led to quick and efficient fallout of precipitation on the windward side of the Cascade Mountains. Caracena *et al.* (1979) concluded that growth by coalescence of drops at low levels made the fallout of rainfall efficient in the Big Thompson Canyon flood of 1976 in the Rocky Mountains.

Superposed epoch analyses of the Doppler-radar data collected in the Lago Maggiore region during autumn 1998 and 1999 indicate that there is a clear relationship between the upstream flow direction and the intensity of precipitation over the Lago Maggiore region. These analyses further show the role of the perpendicularity between the local topography and the airstream. Over the Lago Maggiore region the precipitation was significantly greater when the wind direction around the 2-km level was southerly or southeasterly. The rainfall over the lower slopes rapidly dropped off when the flow became either easterly or westerly. When the southerly and southeasterly flows had a high Froude number, the flow proceeded directly up and over the terrain, and the precipitation was greatly enhanced over the lower windward slopes and over the portions of the Po valley just upstream of the mountains. In extreme cases, this type of flow can lead to flooding in the Alps (Buzzi *et al.* 1998; Doswell *et al.* 1998; Ferretti *et al.* 2000; Rotunno and Ferretti 2001). With low Froude number southerly and southeasterly flows were strongly blocked below the 2-km level. However at higher elevations the airstream rose over the terrain fairly easily. Thus, the enhancement of precipitation directly over the lower mountain slopes was denied the participation of the air in the lowest 2 km, which turned eastward in response to blocking. Apparently the lifting of the low-level air stream was shifted upstream, as precipitation enhancement occurred ~140 km (approximately one Rossby radius) upstream of the barrier crest in the blocked cases.

Composite analysis indicates that the speed of the flow strongly affected whether or not orographic enhancement of the precipitation occurred on the lower windward slopes of the Lago Maggiore region during autumn 1998 and 1999. The role of stability was to determine the location of the precipitation with respect to the topography. When the flow was strong and the stability low, the precipitation was greater over the lower slopes of the Alps and plains close to the mountains. During strong and very stable flow conditions (blocked case), the precipitation was also enhanced but some of the enhancement occurred upstream of the Alps. When the flow was weak the precipitation was in general equal or slightly below the mean, except for the low stability case, when there was some enhancement in the form of patchy cells over the Po valley.

Most of our physical interpretation of the climatological behavior of the Doppler-radar data as a function of upstream wind speed and stability and perpendicularity to the terrain derives from simple basic principles. Stronger wind and lower stability favor flow rising easily over terrain, with most of the precipitation enhancement occurring directly over the lower slopes of the terrain (Fig. 11(c) and (d)). If the stability is low enough, further enhancement may occur by the release of buoyant instability (Fig. 11(a) and (b)). Higher stability favors blocking, which shifts some of the orographic lifting upstream of the mountain barrier (Fig. 11(g) and (h)). These basic principles are discussed ideally in pedagogical references on orographic precipitation (e.g. Smith 1979; Houze 1993). The same principles have been used in various combinations to explain the specific behavior of the Alpine orographic precipitation leading to the famous Piedmont flood of November 1994 (Buzzi *et al.* 1998; Doswell *et al.* 1998; Ferretti *et al.* 2000;

Rotunno and Ferretti 2001). Our study shows how these straightforward basic principles clearly relate to the overall average behavior of the orographic precipitation on the Mediterranean side of the Alps. Moreover, the radar climatology shows that the orographic enhancement is extremely sensitive to the basic upstream flow properties on the detailed scale of the Lago Maggiore region. The upstream flow speed and stability evidently determines whether heavy rains will be directly over the slopes or will be partially shifted upstream, over the Po Valley. Rather slight differences in prevailing upstream wind direction determine on which side of the convex indentation of the Alpine terrain bounding the Lago Maggiore region the heaviest rains and runoff will occur.

Finally, we have found that a diurnal precipitation maximum occurred between 0600 and 0900 UTC over the Lago Maggiore region. To produce this maximum, one may speculate that down-valley flow inside deep river valleys emptying into the larger Po Valley and converging with the synoptic-scale flow in the Po Valley was maximum in the early morning when the air was most stable.

#### ACKNOWLEDGEMENTS

We are grateful to Giamario Galli of the Swiss Meteorological Institute for providing the vast quantities of radar data used in this study. Stacy Brodzik provided engineering support. We also appreciate the scientific advice and comments of Dale Durran, Gianmario Galli, Urs Germann, Dennis Hartmann, Jürg Joss, and Sandra Yuter. Candace Gudmundson edited the manuscript. This research was funded by National Science Foundation grants ATM-9409988 and ATM-9817700 and by an Office of Naval Research grant N00014-97-0717.

#### APPENDIX

In all our maps of rainfall rate and radial velocity, over any given time period or epoch, we apply the Student's  $t$  difference-of-means test at each grid point to indicate the statistical significance of the sample mean. An *a priori* confidence level of 95% rejects the null hypothesis that the mean rainfall rate or radial velocity at a given grid point did not differ significantly from the seasonal mean. Two-sided difference of means tests uses the expression,

$$t = \frac{\bar{x}_1 - \bar{x}_2}{\sqrt{\left( \frac{1}{N_1} + \frac{1}{N_2} \right) \left( \frac{N_1 s_1^2 + N_2 s_2^2}{N_1 + N_2 - 2} \right)}} \quad (5)$$

(Spiegel 1972), where  $\bar{x}_1$ ,  $s_1$  and  $N_1$  are the mean, standard deviation and number of volumes in the sample, and  $\bar{x}_2$ ,  $s_2$  and  $N_2$  are the seasonal mean, standard deviation and total number of volumes in the archive. The null hypothesis is rejected in regions where  $|t| > 1.96$ , corresponding to a 95% confidence level.

The difference-of-means test requires that the volumes in the archive be mutually independent (Wilks 1995). To reduce the statistical dependence between radar samples, we used

a 1-h time interval between successive volume scans. The 1-h time lag reduced the volume-to-volume autocorrelation at each gridpoint to an average of 0.3, with local autocorrelation minima less than 0.1 over the lower terrain and local maxima up to 0.6 in areas where persistent orographic uplift was observed. Because the autocorrelation was higher over the higher terrain, the difference-of-means statistics in these areas may have been quantitatively exaggerated in those regions. In addition, precipitation is a highly skewed quantity; however, the difference-of-means test does not require a Gaussian distribution as long as the sample sizes in all of the analyses are sufficiently large (Wilks 1995). The sample sizes in this study are large enough to meet this condition.

The most informative maps of  $t$ -statistic that we have computed by these methods are discussed where relevant in the body of the paper.

## REFERENCES

- Bougeault, P., P. Binder, A. Buzzi, R. Dirks, R. Houze, J. Kuettner, R. B. Smith, R. Steinacker and H. Volkert, 2001: The MAP Special Observing Period. *Bull. Amer. Meteor. Soc.*, **82**, 433–462
- Bousquet, O., and B. Smull, 2001: Comparative study of two orographic precipitation events exhibiting significant upstream blocking during MAP. MAP Conf., Schliersee, Germany
- Buzzi, A., N. Tartaglione and P. Malguzzi, 1998: Numerical simulations of the 1994 Piedmont flood: Role of orography and moist processes. *Mon. Wea. Rev.*, **126**, 2369-2383
- Cain, D. E., and P. L. Smith, 1976: Operational adjustment of radar estimated rainfall with raingauge data: A statistical evaluation. Preprints, *17<sup>th</sup> Radar Meteorological Conf.*, Seattle, Amer. Meteor. Soc., 533-538
- Caracena, F., R. A. Maddox, L. R. Hoxit and C. F. Chappell, 1979: Mesoanalysis of the Big Thompson Storm. *Mon. Wea. Rev.*, **107**, 1-17
- Chong, M., J.-F. Georgis, O. Bousquet, S. R. Brodzik, C. Burghart, S. Cosma, U. Germann, V. Gouget, R. A. Houze Jr., C. N. James, S. Prieur, R. Rotunno, F. Roux, J. Vivekanandan and Z.-X. Zeng, 2000: Real-time wind synthesis from Doppler-radar observations during the Mesoscale Alpine Programme. *Bulletin of the American Meteorological Society*, **81**, 12, 2953–2962
- Doswell, C. A., C. Ramis, R. Romero and S. Alonso, 1998: A diagnostic study of three heavy precipitation episodes in the western Mediterranean region. *Wea. Forecasting*, **13**, 102-124
- Doviak, R. J., and D. S. Zrnic, 1993: *Doppler Radar and Weather Observations*. 2nd ed. Academic Press, San Diego, 562 pp
- Durrán, D. R., 1990 : Mountain waves and downslope winds. *Atmospheric Processes over Complex Terrain* (W. Blumen, Ed.), American Meteorological Society, Boston, 59-81
- Durrán, D. R., and J. B. Klemp, 1982: On the effects of moisture on the Brunt-Väisälä frequency. *J. Atmos. Sci.*, **39**, 2152-2158
- Ferretti, R., S. Low-Nam and R. Rotunno, 2000: Numerical simulations of the Piedmont flood of 4-6 November 1994. *Tellus*, **52A**, 162-180
- Frei, C., and C. Schär, 1998: A precipitation climatology of the Alps from high-resolution rain-gauge observations. *Int. J. Climatol.*, **18**, 873-900
- Grossman, R. L., and D. R. Durrán, 1984: Interaction of low-level flow with the western Ghat Mountains and offshore convection in the summer monsoon. *Mon. Wea. Rev.*, **112**, 652-672
- Hobbs, P. V., 1975: The nature of winter clouds and precipitation in the Cascade Mountains and their modification by artificial seeding. Part I: Natural conditions. *J. Appl. Meteor.*, **14**, 783-804
- Hobbs, P. V., R. C. Easter and A. B. Fraser, 1973: A theoretical study of the flow of air and fallout of solid precipitation over mountainous terrain. Part II: Microphysics. *J. Atmos. Sci.*, **30**, 813-823
- Houze, R. A., Jr., 1993: *Clouds Dynamics*. Academic Press, 573 pp.
- Houze, R. A., Jr., J. Kuettner and R. B. Smith, 1998: Mesoscale Alpine Programme. U.S. overview document and experiment design. 101 pp. [Available from MAP U.S. Project Office, UCAR/JOSS, P.O. Box 3000, Boulder, CO 80307-3000.]
- Houze, R. A., Jr., S. Medina and M. Steiner, 2000: Two cases of heavy rain on the Mediterranean side of the Alps in MAP. Preprints, *Ninth Conference on Mountain Meteorology*, Aspen, CO, Amer. Meteor. Soc., 1-5

- Houze, R. A., and S. Medina, 2001: Alpine Precipitation Mechanisms in MAP IOP2b and 8. MAP Conf., Schliersee, Germany
- James, C. N., and R. A. Houze, Jr., 2001: An operational four-dimensional Doppler dealiasing scheme. *J. Atmos. Oceanic Technol.*, in press
- James, C. N., S. R. Brodzik, H. Edmon, R. A. Houze, Jr. and S. E. Yuter, 2000: Radar data processing and visualization over complex terrain. *Wea. Forecasting*, **15**, 327-338
- Joss, J., and Coauthors, 1998: Operational use of radar for precipitation measurements in Switzerland. Final Rep. NRP 31, ETH, Zürich, Switzerland, 108 pp
- Joss, J., and A. Waldvogel, 1990: Precipitation measurements and hydrology. *Radar in Meteorology*, Battan Memorial and 40<sup>th</sup> Anniversary Radar Meteorology Conference, (D. Atlas, Ed.), Amer. Meteor. Soc., 577-606
- Kappenberger, G., and J. Kerkmann, 1997: *Il Tempo in Montagna*. Zanichelli Editore S.p.A., Bologna, Italy, 255 pp
- Lionetti, M., 1996: The Italian floods of 4-6 November 1994. *Weather*, **1**, 18-27
- Marshall, J. S., and W. M. Palmer, 1948: The distribution of raindrops with size. *J. Meteor.* **5**, 165-166
- Mass, C. F., and G. K. Ferber, 1990: Surface pressure perturbations produced by an isolated mesoscale topographic barrier. Part I: General characteristics and dynamics. *Mon. Wea. Rev.*, **118**, 2579-2596
- Mohr, C. G., and R. L. Vaughan, 1979: An economical procedure for Cartesian interpolation and display of reflectivity factor data in three-dimensional space. *J. Appl. Meteor.*, **18**, 661-670
- Reed, R. J., and E. E. Recker, 1971: Structure and properties of synoptic-scale wave disturbances in the equatorial western Pacific. *J. Atmos. Sci.*, **28**, 1117-1133
- Rotunno, R., and R. Ferretti, 2001: Mechanisms of intense Alpine rainfall. Submitted, *J. Atmos. Sci.*
- Smith, R. B., 1979: The influence of mountains on the atmosphere. *Adv. Geophys.*, **21**, Academic Press, 87-230
- Spiegel, M. R., 1972: *Schaum's Outline of Theory and Problems of Statistics*. McGraw-Hill, 359 pp.
- Steiner, M., J. A. Smith, B. F. Smull and R. A. Houze, Jr., 2000: Airflow within major river valleys on the south side of the Alps as observed during the MAP special observing period. Preprints, *Ninth Conference on Mountain Meteorology*, Aspen, CO, Amer. Meteor. Soc., 11-14
- Wilks, D. S., 1995: *Statistical Methods in the Atmospheric Sciences*. Academic Press, London, 467 pp

## Figure Captions

**Figure 1.** Mean Alpine precipitation during September- November for 1971 – 1990. Thick lines indicate the 800-m MSL terrain contour. The MAP Northwest Target Area (rectangle) is also shown (After Frei and Schär 1998.)

**Figure 2.** The MAP Northwest Target Area (rectangle). The Swiss-Italian border (white contours), bodies of water (thin contours), geographic features and MAP radar locations are also shown.

**Figure 3.** Vertical cross-section plot of the Cartesian interpolation grid from west to east. The grid points are located where horizontal and vertical lines cross. The Monte Lema radar is located at 0-km range and 1.63-km MSL. The cross-sectional area covered by each 5-min radar volume under standard atmospheric conditions is shaded. The shaded area is determined by the beamwidth of each indicated tilt (expressed in degrees of elevation angle).

**Figure 4.** Constant altitude plots containing the mean radial velocity during all precipitation events observed during 2 MAP seasons by (a) the Monte Lema radar (1998; 554 radar volumes included in calculation) and (b) Monte Lema radar (1999; 598 radar volumes included in calculation). (c-e) RONSARD radar (1999; 213 radar volumes included in calculation). The range ring spacing is 20 km. Note that by Swiss convention, negative (positive) radial velocities denote outbound (inbound) flow.

**Figure 5.** Constant altitude plots at 2-km MSL containing the mean radar-derived rainfall rate observed by the Monte Lema radar during all precipitation events during (a) the 1998 MAP season (554 radar volumes included in calculation) and (b) the 1999 MAP season (598 radar volumes included in calculation). Range ring spacing is 20 km. Vertical cross-section along the red line segment in (a) depicts (c) radar-derived reflectivity and (d) precipitation frequency (i.e. the percentage of volumes for which the reflectivity  $\geq 13$  dBZ at each grid point) during the 1998 MAP season as observed by the Monte Lema radar (554 radar volumes included in calculation). Vertical cross-section along the red line segment in (a) depicts (e) radar-derived reflectivity and (f) precipitation frequency during the 1999 MAP season as observed by the S-Pol radar (320 radar volumes included in calculation). The green contour represents the terrain profile.

**Figure 6.** Constant altitude plots of mean rainfall rates and  $t$ -statistics of rain rate (first and second column, respectively) at 2-km MSL for all precipitation events in which the layer-averaged 925-700 hPa wind in the Milano-Linate sounding indicated flow from (a) and (b)  $67.5$ - $112.5^\circ$  (91 radar volumes included in calculation); (c) and (d)  $112.5$ - $157.5^\circ$  (183 radar volumes included in calculation); (e) and (f)  $157.5$ - $202.5^\circ$  (248 radar volumes included in calculation); and (g) and (h)  $202.5$ - $247.5^\circ$  azimuth (284 radar volumes included in calculation) during the 1998 and 1999 MAP season, along with the 800-m MSL terrain contour. Range ring spacing is 20 km. Red (blue) contours indicate regions where the  $t$ -statistic is greater than or equal to 1.96 (less than or equal to -1.96) and the null hypothesis can be rejected with a 95% confidence level.

**Figure 7.** Mean 2-km fields observed by the Monte Lema radar when the layer-averaged 925-700 hPa flow direction was between  $112.5$ - $202.5^\circ$  azimuth, and the Froude number was  $> 1$ . (a) Rainfall rate and (b)  $t$ -statistic (291 radar volumes included in calculation) and Froude number  $< 1$ . (c) Rainfall rate and (d)  $t$ -statistic (140 radar volumes included in calculation) during the 1998 and 1999 MAP seasons, along with the 800-m MSL terrain contour. Range ring spacing is 20

km. Red (blue) contours indicate regions where the  $t$ -statistic is greater than or equal to 1.96 (less than or equal to -1.96) and the null hypothesis can be rejected with a 95% confidence level.

**Figure 8.** Mean 2-km radial velocity observed by the Monte Lema radar when the layer-averaged 925-700 hPa flow direction was between  $112.5 - 202.5^\circ$  azimuth, and the Froude number was (a)  $> 1$  (291 radar volumes included in calculation) and (b)  $< 1$  (140 radar volumes included in calculation) during the 1998 and 1999 MAP seasons, along with the 800-m MSL terrain contour. Range ring spacing is 20 km. Negative (positive) radial velocities denote outbound (inbound) flow.

**Figure 9.** Mean 0.5-km radial velocity observed by the RONSARD radar when the layer-averaged 925-700 hPa flow direction was between  $112.5-202.5^\circ$  azimuth, and the Froude number was (a)  $> 1$  (72 radar volumes included in the calculation) and (b)  $< 1$  (52 radar volumes included in the calculation) during the 1999 MAP season, along with the 800-m MSL terrain contour. Range ring spacing is 20 km. Negative (positive) radial velocities denote outbound (inbound) flow.

**Figure 10.** Mean fields observed by the RONSARD radar when the layer-averaged 925-700 hPa flow direction was between  $112.5-202.5^\circ$  azimuth and the Froude number was  $> 1$ . (a) 2-km rainfall rate (b) 2-km  $t$ -statistics and (c) vertical cross-section along the red line in (a) of the precipitation frequency (72 radar volumes included in the calculation); and for Froude number  $< 1$ . (d) 2-km rainfall rate, (e) 2-km  $t$ -statistics and (f) vertical cross-section along the red line in (a) of the precipitation frequency (52 radar volumes included in the calculation) during the 1999 MAP season. Range ring spacing is 20 km. Red (blue) contours indicate regions where the  $t$ -statistic is greater than or equal to 1.96 (less than or equal to -1.96) and the null hypothesis can be rejected with a 95% confidence level.

**Figure 11.** Mean 2-km rainfall rate and  $t$ -statistic (first and second columns) observed by the Monte Lema radar when the layer-averaged 925-700 hPa flow direction was between  $112.5-202.5^\circ$  azimuth, and the Froude number was  $> 1$  for (a) and (b) flow below  $8 \text{ m s}^{-1}$  (121 radar volumes included in calculation) and (c) and (d) flow above  $8 \text{ m s}^{-1}$  (68 radar volumes included in calculation) and Froude number  $< 1$  for (e) and (f) flow below  $8 \text{ m s}^{-1}$  (170 radar volumes included in calculation) and (g) and (h) flow above  $8 \text{ m s}^{-1}$  (72 radar volumes included in calculation) during the 1998 and 1999 MAP seasons, along with the 800-m MSL terrain contour. Range ring spacing is 20 km. Red (blue) contours indicate regions where the  $t$ -statistic is greater than or equal to 1.96 (less than or equal to -1.96) and the null hypothesis can be rejected with a 95% confidence level.

**Figure 12.** Total Monte Lema radar-derived rainfall estimate by the hour over the Northwest Target Area (rectangle in Figs. 1 and 2) at an altitude of 2-km MSL during (a) the autumn 1998 and (b) autumn 1999 MAP seasons.

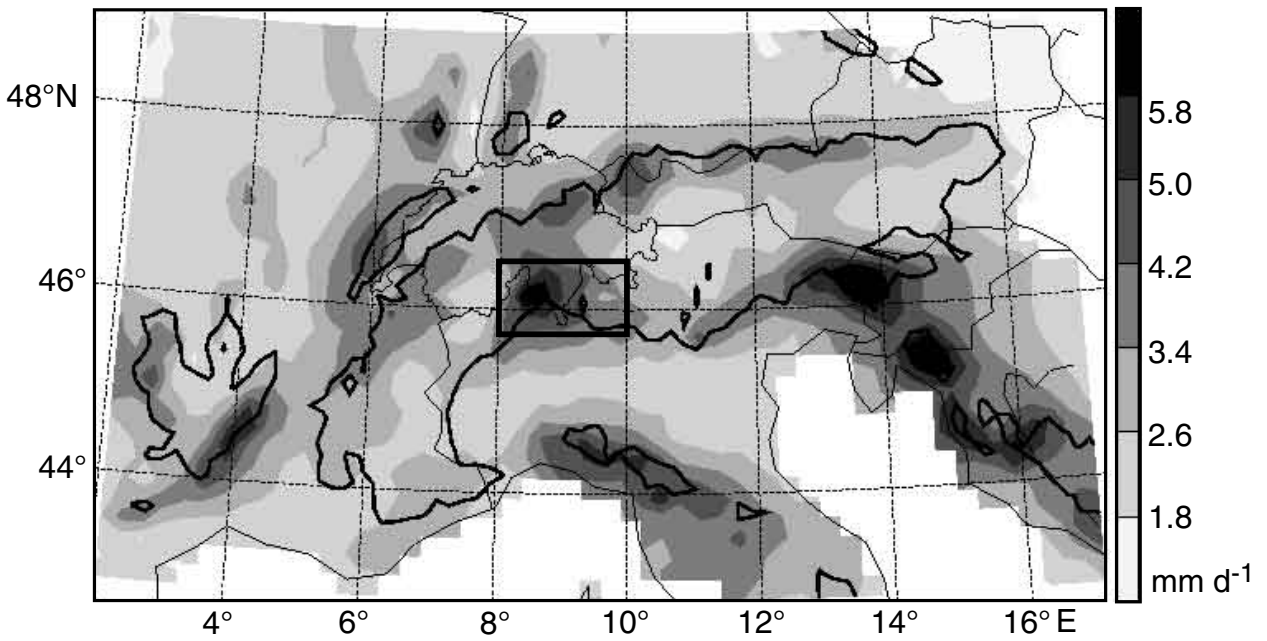


**Figure 1.** Mean alpine precipitation during September-November 1971-1990. Thick lines indicate the 800-m MSL terrain contour. The MAP Northwest Target Area (rectangle) is also shown (After Frei and Schär 1998.)

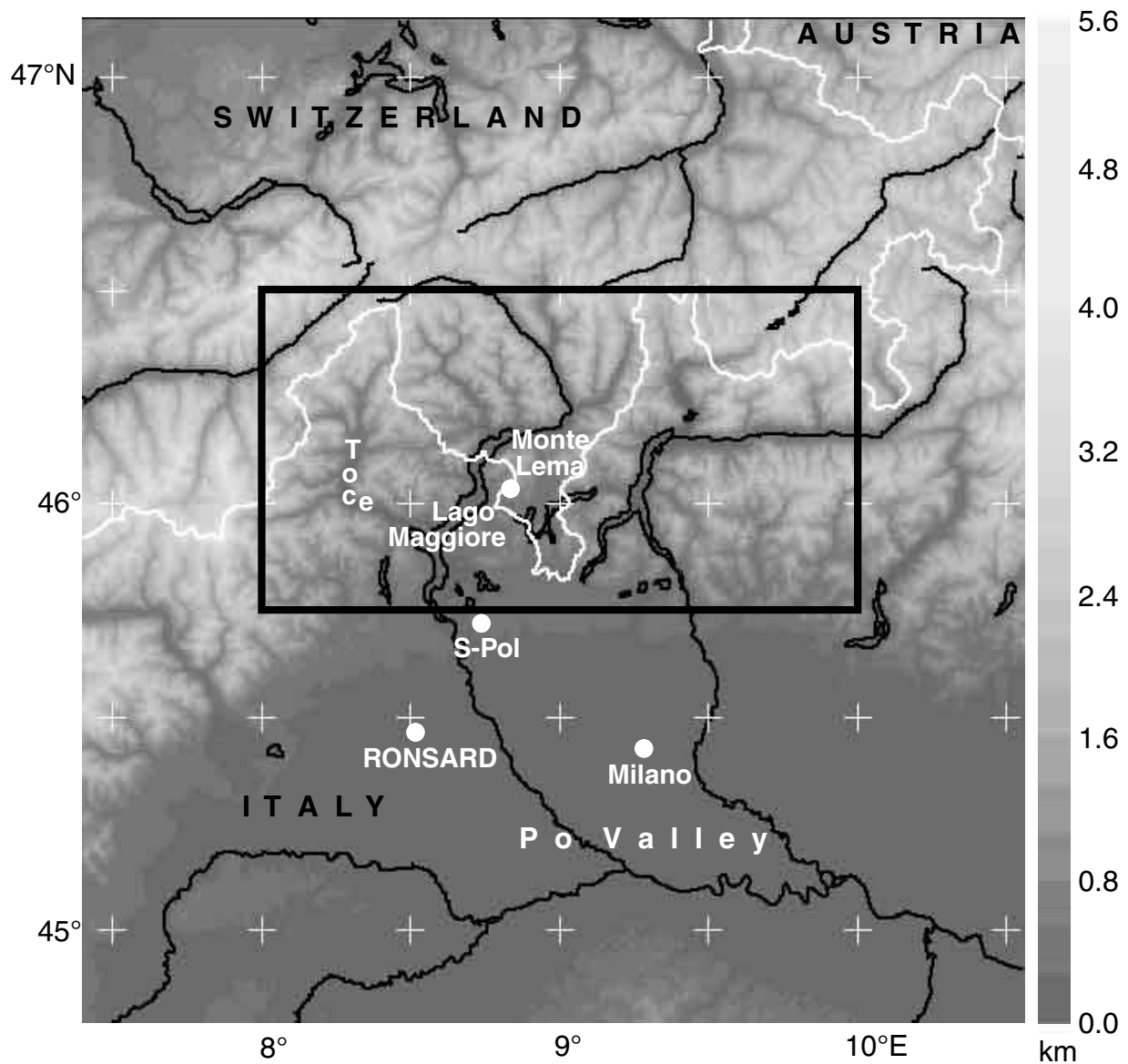


**Figure 2.** The MAP Northwest Target Area (rectangle). The Swiss-Italian border (white contour) bodies of water (thin contours), geographic features, and MAP radar locations are also shown.

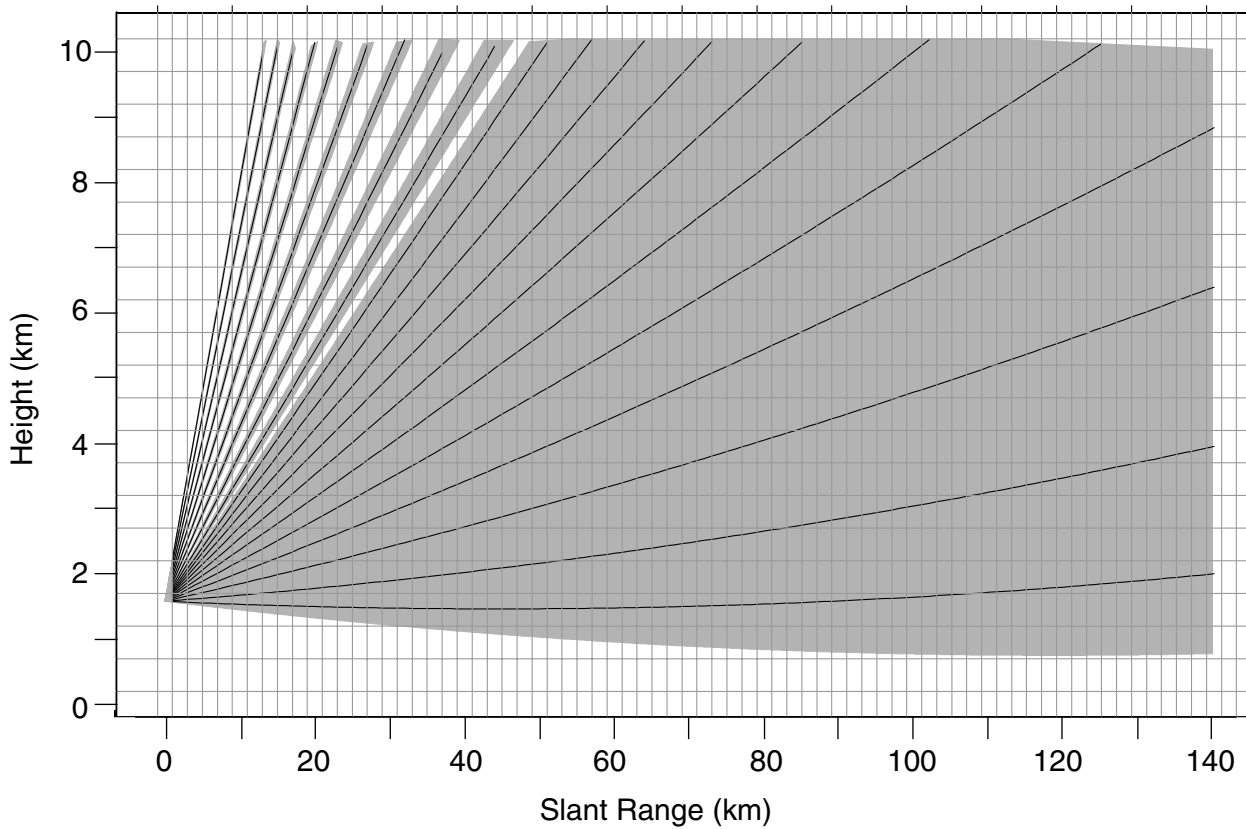


**Figure 3.** Vertical cross-section plot of the Cartesian interpolation grid from west to east. The grid points are located where horizontal and vertical lines cross. The Monte Lema radar is located at 0-km range and 1.63-km MSL. The cross-sectional area covered by each 5-min radar volume under standard atmospheric conditions is shaded. The shaded area is determined by the beamwidth of each indicated tilt (expressed in degrees of elevation angle).

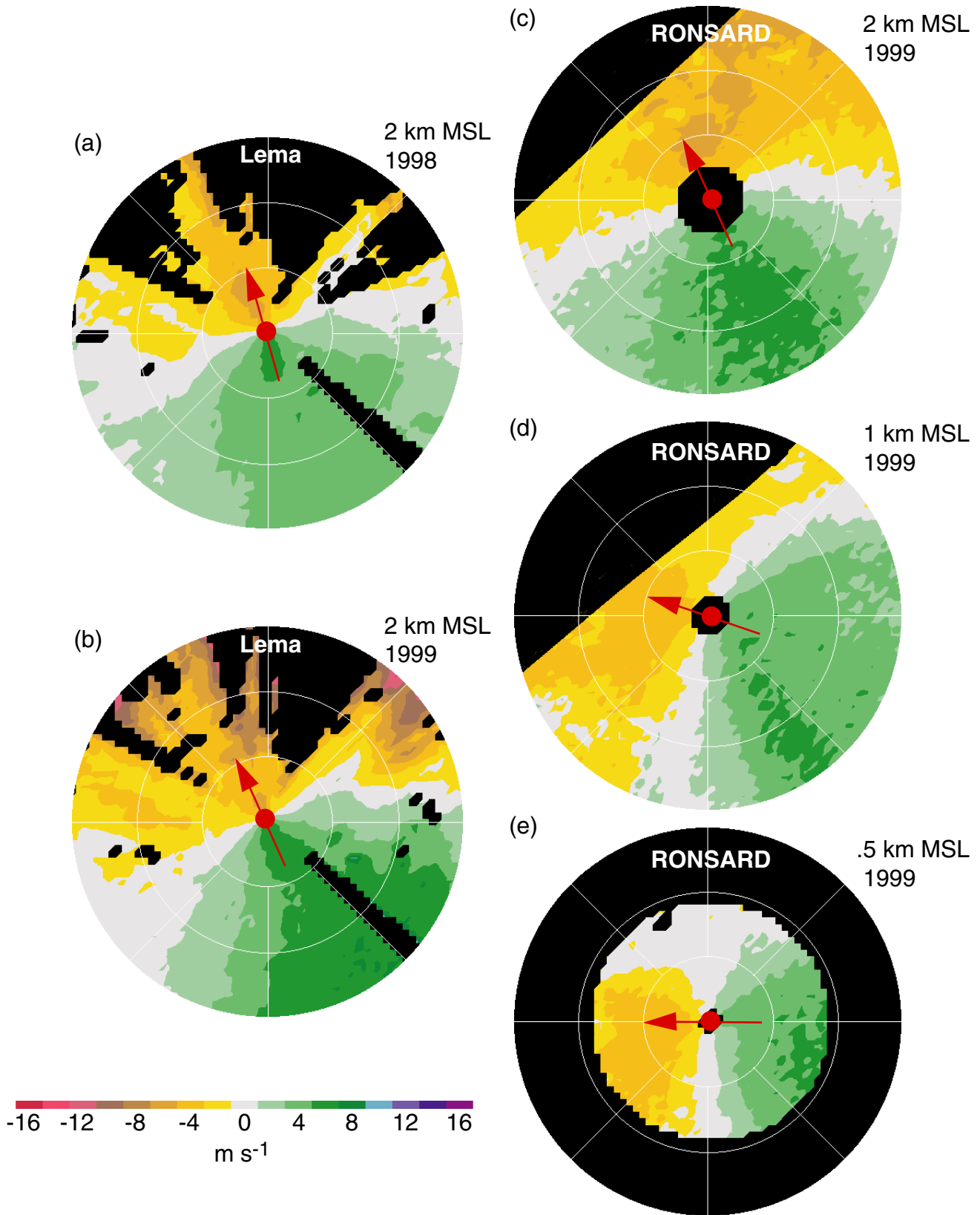


**Figure 4.** Constant altitude plots containing the mean radial velocity during all precipitation events observed during 2 MAP seasons by (a) the Monte Lema radar (1998; 554 radar volumes included in the calculation). (b) Monte Lema radar (1999; 598 volumes included in the calculation). (c-e) RONSARD radar (1999; 213 volumes included in the calculation). Range ring spacing is 20 km. Note that by Swiss convention, negative (positive) radial velocities denote outbound (inbound) flow.

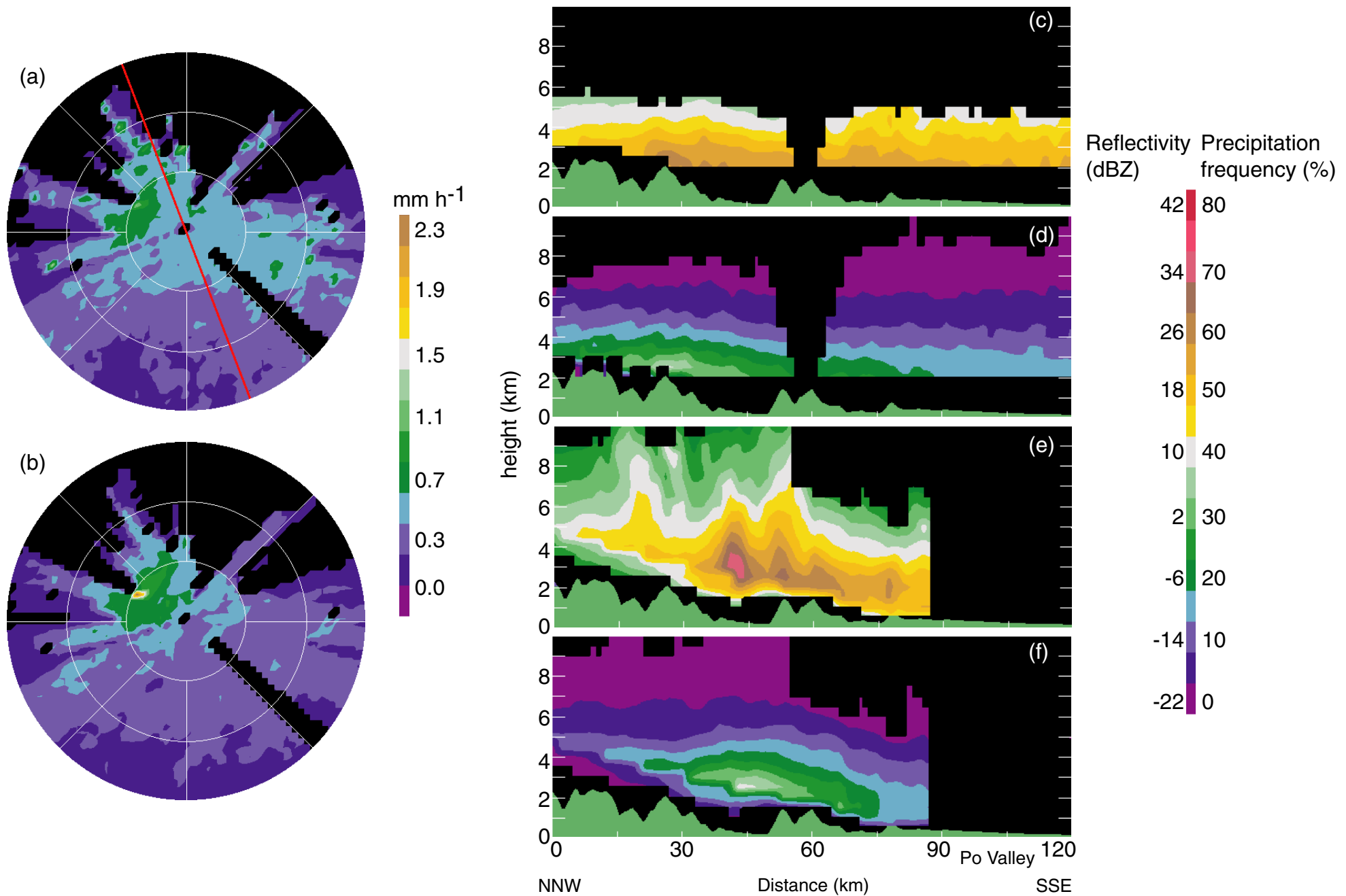


**Figure 5.** Constant altitude plots at 2-km MSL containing the mean radar-derived rainfall rate observed by the Monte Lema radar during all precipitation events during the (a) 1998 MAP season (554 radar volumes included in the calculation) and (b) 1999 MAP season (598 radar volumes included in the calculation). Range-ring spacing is 20 km. Vertical cross-section along the red line in (a) depicts (c) radar-derived reflectivity and (d) precipitation frequency (i.e., the percentage of volumes for which the reflectivity  $\geq 13$  dBZ at each grid point) during the 1998 MAP season as observed by the Monte Lema radar (554 radar volumes included in the calculation). Vertical cross-section along the red line segment in (a) depicts (e) radar-derived reflectivity and (f) precipitation frequency during the 1999 MAP season as observed by the S-Pol radar (320 radar volumes included in the calculation). The green contour represents the terrain profile.

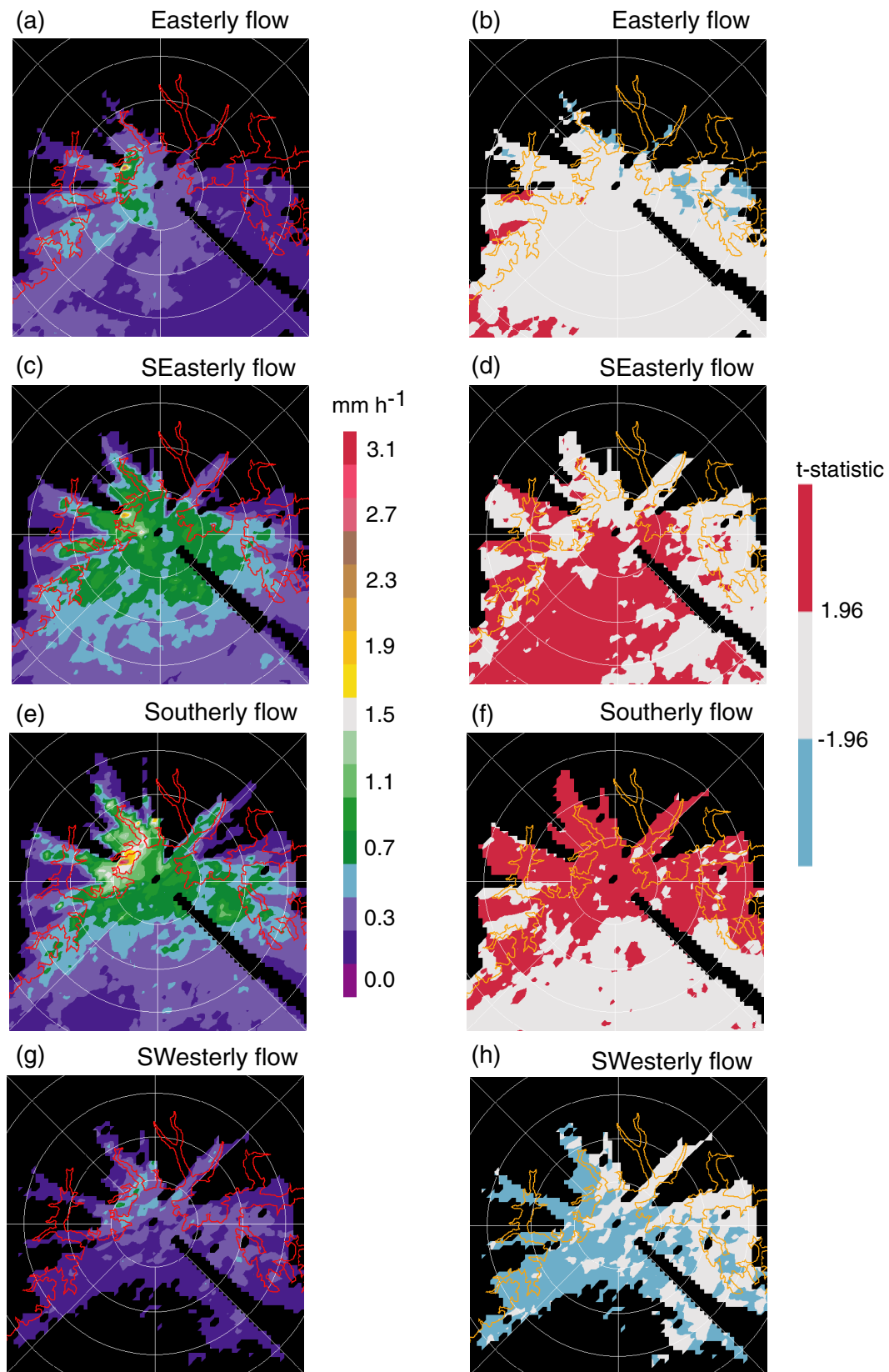


**Figure 6.** Constant altitude plots of mean rainfall rates and  $t$ -statistic of rain rate (first and second column, respectively) at 2-km MSL for all precipitation events in which the layer-averaged 925-700 hPa wind in the Milano-Linate sounding indicated flow from (a) and (b) 67.5-112.5° (91 radar volumes included in calculation); (c) and (d) 112.5-157.5° (183 radar volumes included in calculation); (e) and (f) 157.5-202.5° (248 radar volumes included in calculation); and (g) and (h) 202.5-247.5° azimuth (284 radar volumes included in calculation) during the 1998 and 1999 MAP season, along with the 800-m MSL terrain contour. The range ring spacing is 20 km. Red (blue) contours indicate regions where the  $t$ -statistic is greater than or equal to 1.96 (less than or equal to -1.96) and the null hypothesis can be rejected with a 95% confidence level.

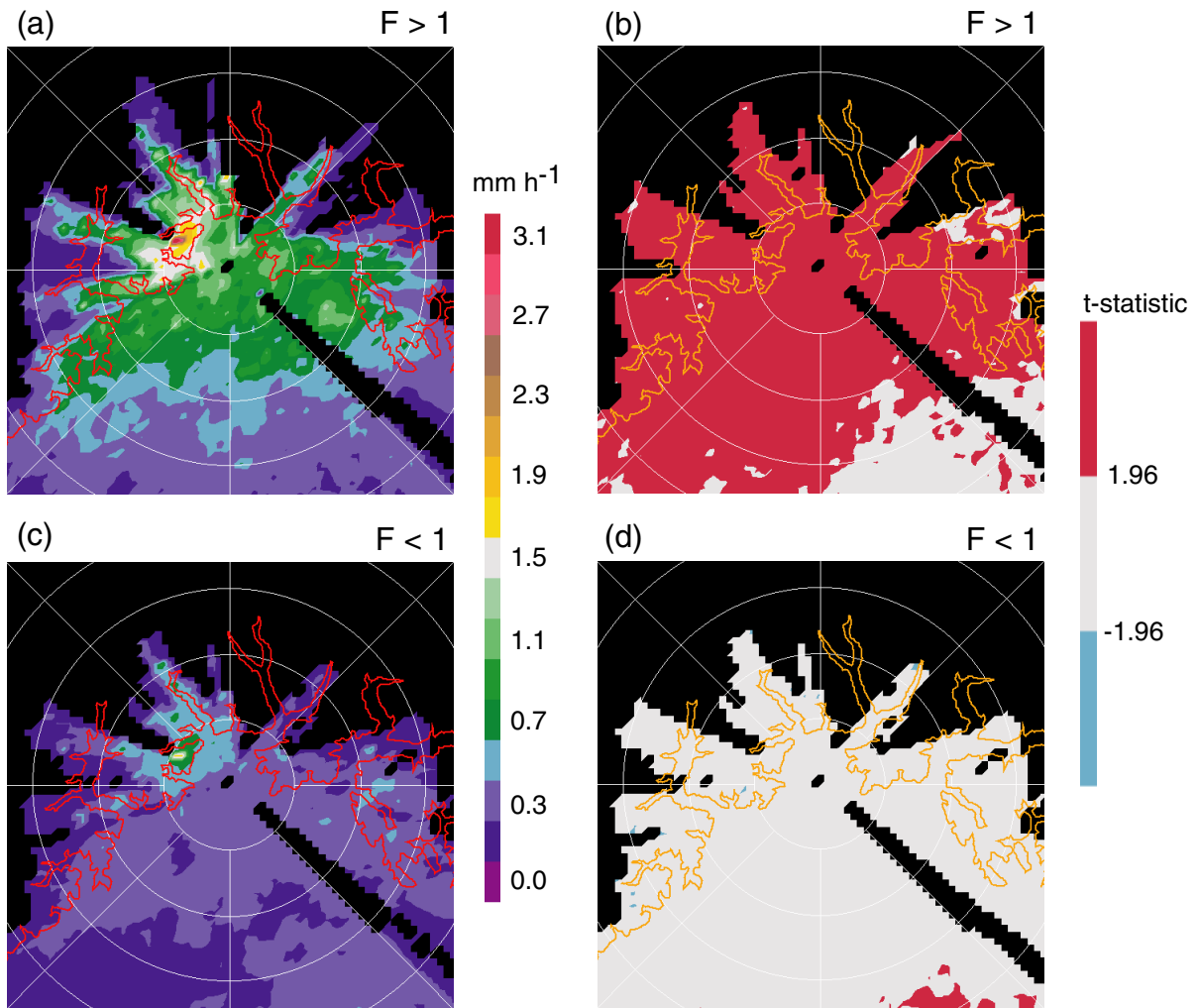


**Figure 7.** Mean 2-km fields observed by the Monte Lema radar when the layer-averaged 925-700 hPa flow direction was between 112.5-202.5° azimuth, and the Froude number was > 1. (a) Rainfall rate and (b)  $t$ -statistic (291 radar volumes included in calculation) and the Froude number was < 1. (c) Rainfall rate and (d)  $t$ -statistic (140 radar volumes included in the calculation) during the 1998 and 1999 MAP seasons, along with the 800-m MSL terrain contour. The range ring spacing is 20 km. Red (blue) contours indicate regions where the  $t$ -statistic is greater than or equal to 1.96 (less than or equal to -1.96) and the null hypothesis can be rejected with a 95% confidence level.

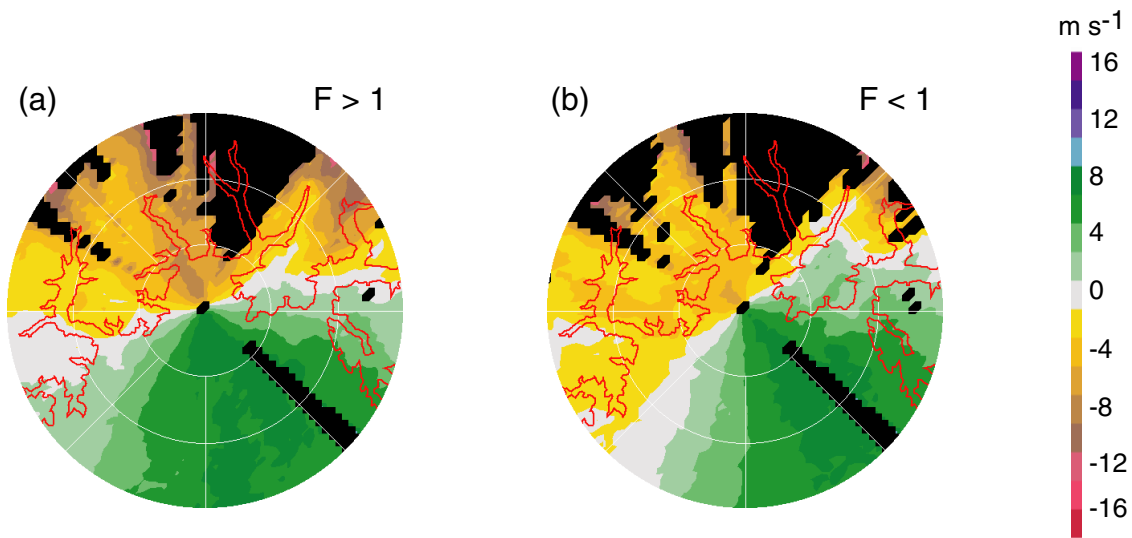


**Figure 8.** Mean 2-km radial velocity observed by the Monte Lema radar when the layer-averaged 925-700 hPa flow direction was between 112.5-202.5° azimuth, and the Froude number was (a)  $> 1$  (291 radar volumes included in the calculation) and (b)  $< 1$  (140 radar volumes included in the calculation) during the 1998 and 1999 MAP seasons, along with the 800-m MSL terrain contour. The range ring spacing is 20 km. Negative (positive) radial velocities denote outbound (inbound) flow.

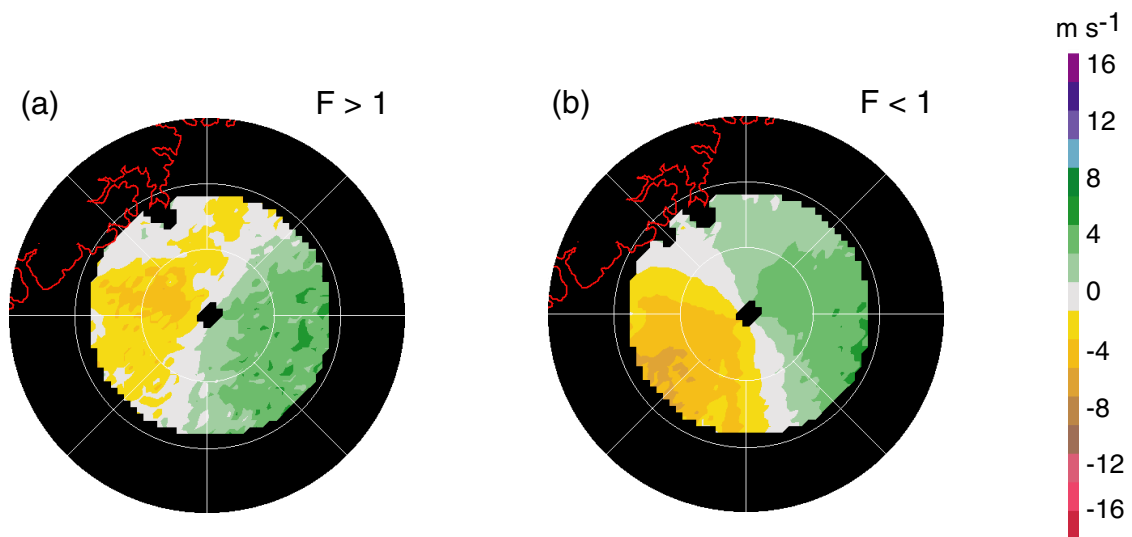


**Figure 9.** Mean 0.5-km radial velocity observed by the RONSARD radar when the layer-averaged 925-700 hPa flow direction was between 112.5-202.5° azimuth, and the Froude number was (a)  $> 1$  (72 radar volumes included in the calculation), and (b)  $< 1$  (52 radar volumes included in the calculation) during the 1999 MAP season, along with the 800-m MSL terrain contour. The range ring spacing is 20 km. Negative (positive) radial velocities denote outbound (inbound) flow.

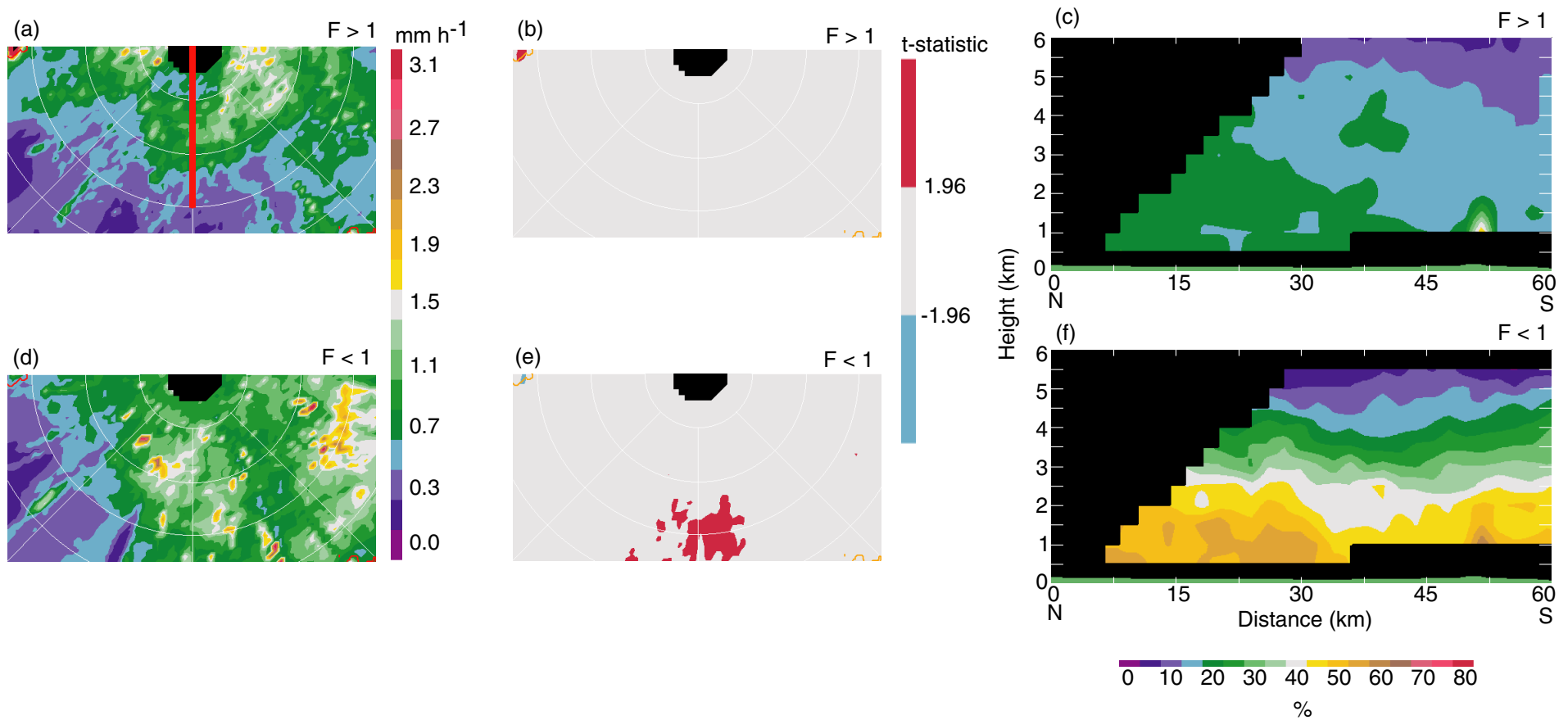


**Figure 10.** Mean fields observed by the RONSARD radar when the layer-averaged 925-700 hPa flow direction was between 112.5-202.5° azimuth, and the Froude number was  $> 1$ . (a) 2-km rainfall rate, (b) 2-km  $t$ -statistics, and (c) vertical cross-section along the red line in (a) of the precipitation frequency (72 radar volumes included in the calculation) and for Froude number  $< 1$ . (d) 2-km rainfall rate, (e) 2-km  $t$ -statistics, and (f) vertical cross-section along the red line in (a) of the precipitation frequency (52 radar volumes included in the calculation) during the 1999 MAP season. The range ring spacing is 20 km. Red (blue) contours indicate regions where the  $t$ -statistic is greater than or equal to 1.96 (less than or equal to -1.96) and the null hypothesis can be rejected with a 95% confidence level.

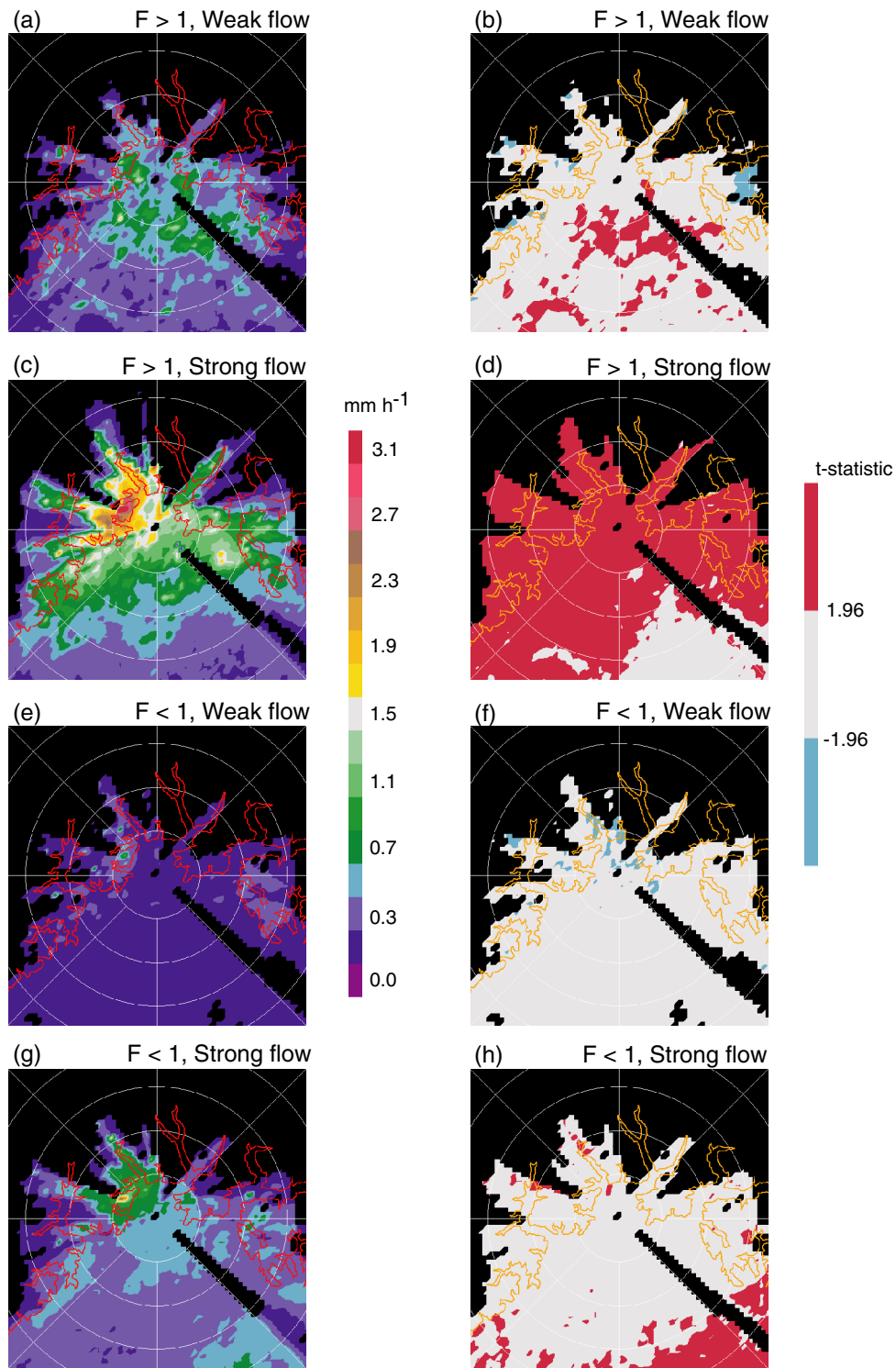


**Figure 11.** Mean 2-km rainfall rate and  $t$ -statistic (first and second columns) observed by the Monte Lema radar when the layer-averaged 925-700 hPa flow direction was between  $112.5\text{-}202.5^\circ$  azimuth, and the Froude number was  $> 1$  for (a) and (b) flow below  $8\text{ m s}^{-1}$  (121 radar volumes included in calculation) and (c) and (d) flow above  $8\text{ m s}^{-1}$  (68 radar volumes included in the calculation) and Froude number  $< 1$  for (e) and (f) flow below  $8\text{ m s}^{-1}$  (170 radar volumes included in the calculation) and (g) and (h) flow above  $8\text{ m s}^{-1}$  (72 radar volumes included in the calculation) during the 1998 and 1999 MAP seasons, along with the 800-m MSL terrain contour. The range ring spacing is 20 km. Red (blue) contours indicate regions where the  $t$ -statistic is greater than or equal to 1.96 (less than or equal to -1.96) and the null hypothesis can be rejected with a 95% confidence level.

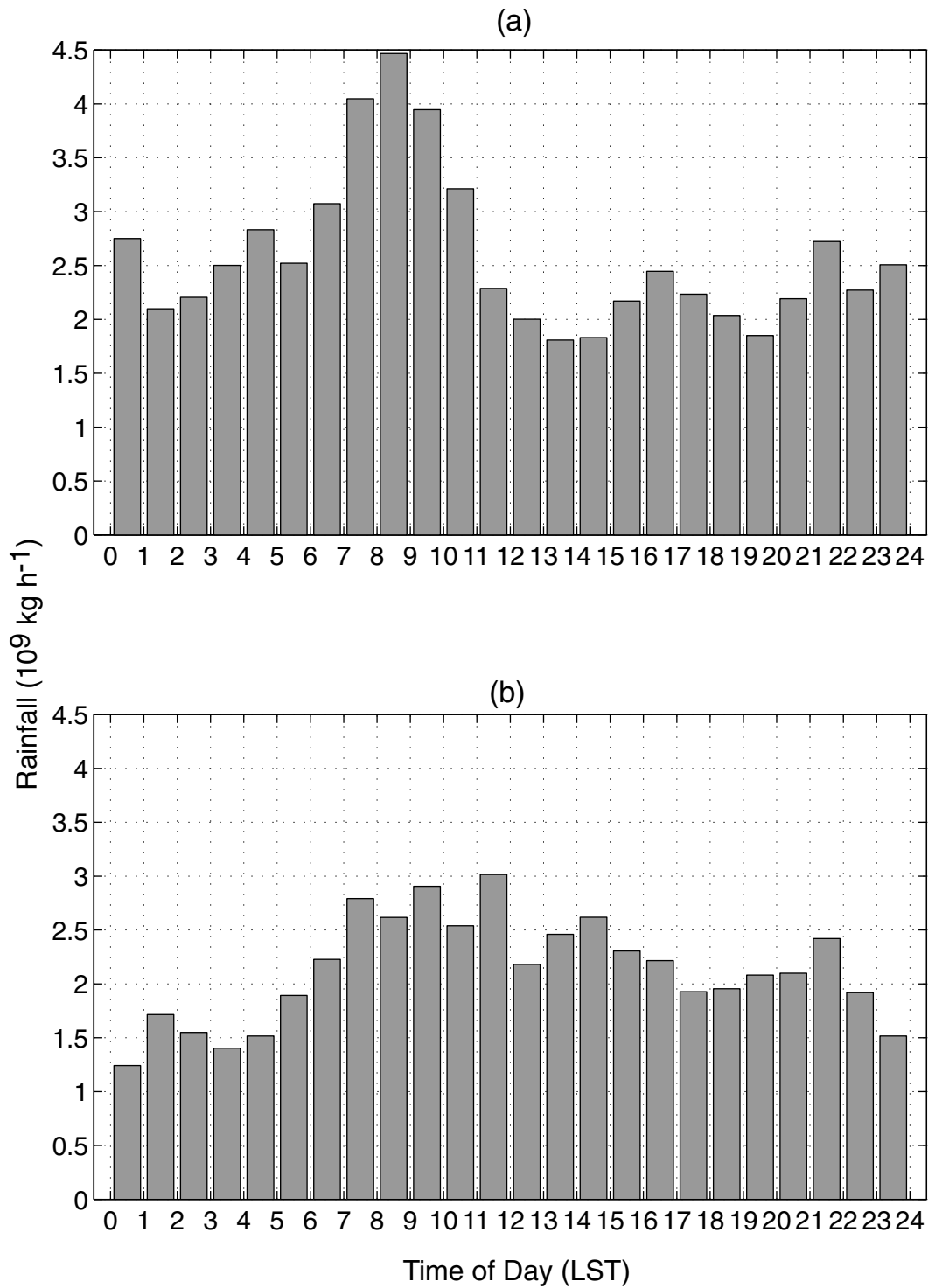


**Figure 12.** Total Monte Lema radar-derived rainfall estimate by the hour over the Northwest Target Area (rectangle in Figs. 1 and 2) at an altitude of 2-km MSL during (a) the autumn1998 and (b) autumn1999 MAP seasons.